Photoelectrocatalytic conversion of urea under solar illumination using Ni decorated Ti-Fe2O3 electrodes

Lamia Rebiai, Diane Muller-Bouvet, Raihana Benyahia, Encarnación Torralba, Melissa Lopez Viveros, Vincent Rocher, Sam Azimi, Christine Cachet-Vivier, Stéphane Bastide

Photoelectrocatalytic conversion of urea under solar illumination using Ni decorated Ti-Fe_2O_3 electrodes

Lamia Rebiai[1], Diane Muller-Bouvet[1], Raihana Benyahia[1], Encarnación Torralba[1], Melissa Lopez Viveros[2], Vincent Rocher[2], Sam Azimi[2], Christine Cachet-Vivier[1], Stéphane Bastide[1*]

[1] University of Paris Est, ICMPE (UMR 7182), CNRS, UPEC, F-94320 Thiais, France.

[2] Greater Paris Sanitation Authority (SIAAP), Direction of Innovation, 82 avenue Kléber, F-92700, Colombes, France

*** Author for correspondence:** Dr. Stéphane Bastide, stephane.bastide@cnrs.fr
Institut de Chimie et des Matériaux Paris-Est
2 rue Henri Dunant, 94320 Thiais, France

Highlights

- Urea conversion with Fe_2O_3/Ni photoelectrodes as substitute for N-removal in WWTPs
- Anodic photoelectrodeposition of NiOOH on n-Fe_2O_3 nanorods where h^+ are collected
- Gain of 0.5 V in urea oxidation onset potential with FTO/Ti-Fe_2O_3/Ni *vs.* Ni electrode
- *In situ* light transmission recorded during CV confirms urea oxidation as EC process
- Urea PEC conversion leads to N_2, O_2, and NO_2^- ; FE ~ 10-20% for N removal as N_2

Keywords: photoelectrocatalysis, urea, nitrogen remediation, hematite, nickel hydroxide

Abstract

To reduce the energy cost and environmental impact of biological nitrogen removal in wastewater treatment plants, it would be advantageous to treat urea contained in urine at the source. In this perspective, FTO/Ti-Fe_2O_3 (nanorods) photoelectrodes decorated with Ni as catalyst are developed and tested for urea photoelectrocatalytic oxidation under solar illumination. Gains up to 0.50 V in oxidation onset potential *vs.* metallic Ni are obtained thanks to a Ni photoelectrodeposition method. *In situ* transmission measurements (based on NiOOH light absorption) during electrochemical cycling allowed to evaluate the state of active Ni sites and confirmed that urea oxidation mechanism is of EC type. Photoelectrolyses give faradaic efficiencies of 10-18% and 9-35% for N_2 and O_2 formation, respectively. A significant and unexpected NO_2^- production (~65%) is detected indicating another or incomplete reaction pathway. The photoelectrocatalytic removal of nitrogen from urea solutions is demonstrated but requires catalysts with higher selectivity towards N_2.

1. Introduction

In wastewater treatment plants (WWTPs), the biological treatment used for nitrogen removal nowadays faces a couple of challenges. On one hand, it is a large consumer of electricity, with up to 60% of the electrical consumption of a conventional WWTP [1]. In Ile-de-France region, recent operational data from the Greater Paris Sanitation Authority (SIAAP) show that it is the first energy item with 30% of the total electrical consumption of Seine Aval WWTP (260 GWh, 6 M inhabitants) [2].

The main source of nitrogen received in WWTPs is urea contained in urine (80%). Relocating part of the nitrogen treatment would reduce the economic and ecological footprint (by reducing the production of N_2O) and partially meet the challenges of growing demography. Alternative elimination processes based on selective urine collection and electrooxidation [3],[4],[5],[6] or photoelectrooxidation of urea have been proposed following the first works of G. Botte *et al.* in 2009 [7]. Remediation of urea at the photoanode is coupled to H_2 production at the cathode, in an alkaline medium, according to the following reaction:

$$CO(NH_2)_2 + H_2O + E_{solar}\,(h\nu) + E_{electrochemical}\,(\Delta V) \rightarrow CO_2 + N_2 + 3\,H_2 \qquad (R1)$$

This reaction must be carried out using a nickel-based electrocatalyst ($Ni(OH)_2$) and in an alkaline medium. In theory, it allows the elimination of nitrogen from the solution (urine) in the form of N_2 (gas without greenhouse effect). Furthermore, the production of H_2 from R1 theoretically requires three times less energy than from water electrolysis (thermodynamic cell voltage of 0.37 V_{RHE} *vs.* 1.23 V_{RHE}, respectively) [7]. The vast untapped resource of urea in urine (60 Mt/year in humans) thus makes the R1 reaction very attractive, both to avoid the energy and environmental cost of biological treatment in WWTPs, and to produce H_2 potentially more efficiently than by electrolysis of water.

To our knowledge, only a few works have been devoted to the photoelectrooxidation of urea, as reported by Zhu *et al.* in a recent review [8]. The main interest is to use solar energy to decrease the oxidation potential of urea due to the photopotential generated in a semiconductor (n-type) under illumination [9–12]. In these studies, hematite is commonly chosen as it offers highly suitable characteristics: it is inexpensive to synthesize, non-toxic and stable at high pH, which is a prerequisite because the only effective catalysts for urea oxidation are based on the $Ni(OH)_2$/NiOOH couple which only works at high pH. Moreover, hematite is naturally n-type and absorbs light in the visible range (Eg ~ 2.1 eV), giving a theoretical maximum photocurrent of 12 mA cm^{-2} under AM1.5 solar illumination [13]. Lastly, there is a hydrothermal method for the synthesis of hematite nanowires well adapted for photoelectrochemistry [14], which has given rise to an abundant literature [15,16].

Wang *et al.* were the first to propose the formation of H_2 by photoelectrooxidation of urea and urine under solar illumination. They studied in an alkaline medium TiO_2 and Fe_2O_3 electrodes on

which $Ni(OH)_2$ is deposited by a dip-coating method [9]. They showed a decrease in the oxidation potential of urea with hematite from 1.36 V_{RHE} in the dark to 0.91 V_{RHE} under solar illumination. After the addition of $Ni(OH)_2$ as a catalyst, the onset potential is further shifted from -400 mV (0.51 V_{RHE}) and the photocurrent increases substantially to ~1.5 mA cm^{-2} at 1.23 V_{RHE}. They also showed that voltammograms obtained in urine are similar to those obtained in urea solutions.

Xu *et al.* [10] obtained by hydrothermal synthesis, titanium-doped hematite (Ti-Fe_2O_3) nanowires which are decorated with $Ni(OH)_2$ by cathodic electrodeposition in an aqueous $Ni(NO_3)_2$ solution. They studied the influence of the electrodeposition time on the photoelectrochemical performances and showed that the presence of the catalyst (optimized in thickness) induced a shift of ~ -100 mV in the voltammograms, with a onset potential of urea oxidation at 0.7 V_{RHE} under illumination against 1.35 V_{RHE} for urea electrolysis (without photo assistance), representing a gain of 0.65 V. Accordingly, the photocurrent (at 1.3 V_{RHE}) increases from ~0.3 mA cm^{-2} (Ti-Fe_2O_3 alone) to ~1.6 mA cm^{-2} after adding $Ni(OH)_2$.

More recently, Gan *et al.* [12] measured a photocurrent of 5 mA cm^{-2} in a urea solution and 7.5 mA cm^{-2} in human urine, using arrays of Co-doped Fe_2O_3 nanowires deposited on flexible support and functionalized by Au nanoparticles. $Ni(OH)_2$ is deposited using a dip-coating method. Au and $Ni(OH)_2$ eventually act as plasmonic nanostructures. They obtained a continuous H_2 release at the cathode under low polarization (1.23 V_{RHE}).

The efficiency of coupling Fe_2O_3 and Ni catalysts is crucial in these systems. It depends on the deposition method, the initially deposited species (Ni^0, $Ni(OH)_2$), the thickness, the coverage rate of nanowires, and the defects present at the interface (recombination). In this work, we explored two alternative methods: Ni^0 sputtering and NiOOH anodic photoelectrodeposition, which have been recently studied with Fe_2O_3 for the photoelectrooxidation of water. Sputtering is a physical method that is simple to implement and allows to obtain deposits of controlled thickness [17,18]. The anodic photoelectrodeposition is particularly well adapted to an n-type semiconductor [19–21], it is expected to occur where the charges (h^+) are generated and collected along the nanowires.

We studied the properties of Fe_2O_3/Ni photoanodes for the photoelectrooxidation of water and urea and tried to clarify the proportion of these two competing reactions. We also attempted to determine whether the photopotential induced under illumination indeed allows the oxidation of $Ni(OH)_2$ to NiOOH at lower potentials, which is the basis of the accepted EC mechanism for the electrooxidation of urea on Ni [22]:

$$Ni^{II}(OH)_2 + OH^- \rightarrow Ni^{III}OOH + H_2O + e^- \quad (E)$$

$$CO(NH_2)_2 + 6\ NiOOH + H_2O \rightarrow 6\ Ni(OH)_2 + N_2 + CO_2 \quad (C)$$

For this purpose, we performed *in situ* light transmittance measurements taking advantage of the differences in optical absorption of $Ni(OH)_2$ and NiOOH in the visible spectrum.

Lastly, previous studies reported in the literature were focused on the production of hydrogen at the cathode, the anodic reaction mechanism being usually assumed to be R1, *i.e.*, without analysis of the products formed. Our primary goal being the removal of nitrogen from the liquid phase (preferably in N_2 gas), we sought to determine the gaseous as well as the dissolved products of the reaction and to calculate a faradaic efficiency for each product after photoelectrolyses of several hours.

2. Methods and Materials

2.1 Elaboration of photoelectrodes

Fe_2O_3 films are deposited by a hydrothermal method on the FTO substrates (Fluorine doped Tin Oxide) provided by Visiontech-Systems (FTO Glass Tech7, 600 nm thick FTO layer on 2 mm thick glass substrate, 7 ohms/square, 1.8 cm x 5.0 cm). Glass/FTO substrates are first cleaned by sonication for 10 min in water + soap, then for 10 min in ethanol and 10 min in acetone. This procedure is repeated a second time and the substrates are eventually sonicated in deionized water for 20 min. Afterward, Fe_2O_3 is deposited on the substrates according to a hydrothermal method inspired from Chen and Chen's work **[23]**. The glass/FTO substrates are immerged in a PTFE container filled with 25 mL of water (18 Mohm.cm, Millipore), 0.05 mol L^{-1} $FeCl_3$ (VWR, 99.3%), 0.50 mol L^{-1} of $NaNO_3$ (Merck, 99.5%) and 50 µL of HCl (VWR, 37 %). The container is placed in an oven and heated at 100°C for 6 hours. The obtained iron oxyhydroxide (FeOOH) is then annealed at 550°C for 1 hour and 800°C for 20 min (ramp rate of 4°C min^{-1}) to form Fe_2O_3 ($2FeOOH \rightarrow Fe_2O_3 + H_2O$).

The samples are doped with titanium by adding $TiCl_4$ (Merck, liquid, 97%) in the hydrothermal synthesis solution at a concentration of 0.5 $\%_{vol}$ [23]. These samples are referred to as Ti-Fe_2O_3.

An active surface of 4 cm^2 is delimited with an electrolytic tape for further electrochemical studies or treatments.

2.2 Nickel deposition

Two methods have been used to deposit Ni in the metallic or oxidized state on hematite, respectively by sputtering or by photoelectrochemical (PEC) anodic deposition.

In the first case, Ni^0 deposition is performed with a Cressington 208 HR sputter, at 0.3 bar argon pressure and 60 mA, using a Ø57 mm nickel target (99.98%, Ted Pella, Inc). The thickness of the layer is monitored by a quartz crystal microbalance.

In the second case, a photoelectrodeposition method inspired by Tamirat [21] and Malara [20] is applied to obtain NiOOH according to the anodic reaction with h^+ photogenerated in Ti-Fe_2O_3:

$$Ni^{2+}_{(aq)} + h^+ + 3\ OH^- \rightarrow NiOOH + H_2O$$

FTO/Ti-Fe_2O_3 samples are immersed in 100 mL of an aqueous solution containing 10 mmol L^{-1} $NiSO_4.6\ H_2O$ (Alfa Aesar, 98%) and 30 mmol L^{-1} $(NH_4)_2SO_4$ (VWR, 99.5%). The pH is adjusted to 9 by adding ammonia to the solution [24]. The coating was performed under AM1.5G solar illumination

by chronoamperometry at 1.23 V_{RHE}, the amount deposited being controlled by the charge transferred. A voltammogram and a chronoamperogram corresponding to the coating process are presented in Figure S1 in the Supplementary Information (SI).

The photoelectrodes are electrochemically cycled several times in a 1 mol L^{-1} NaOH solution to obtain a stable intensity of $Ni(OH)_2$/NiOOH peaks (see Figure S2 in SI). The electrodes are referred to as FTO/Ti-Fe_2O_3/Ni_{SP} and FTO/Ti-Fe_2O_3/Ni_{PEC} depending on the type of deposition method.

We tested different amounts of Ni deposit by both methods. The optimum in terms of photoelectrochemical response for urea oxidation is 2 nm for sputtering and 8.75 mC cm^{-2} for PEC deposition, as shown in Figures S3 and S4 in SI.

2.3 Physical characterization

Structural characterization was performed by X-ray diffraction (XRD) using a Bruker D8 Advanced diffractometer (Cu K radiation). The morphology of the Ti-Fe_2O_3 layers was observed by scanning electron microscopy (SEM) with a Zeiss Merlin FEG microscope equipped with an InLens detector, at an accelerating voltage of 5-15 kV. Energy-dispersive X-ray spectroscopy used to identify elements was performed with an AZtec EDS Advanced system (HKL Nordlys Nano, Oxford Instruments), equipped with an X-Max SDD detector and at an accelerating voltage of 10-15 kV.

2.4 Optical properties

Optical measurements were performed using a Hitachi U-41000 spectrophotometer, incorporating two light sources: a deuterium lamp in the UV (100 - 400 nm) and a halogen lamp in the visible/near IR (400 - 850 nm). Using an integrating sphere, the total transmittance *T* and reflectance *R* are measured *vs.* wavelength λ. The absorptance spectrum *A* is calculated according to $A = 1 - T - R$.

2.5 Photoelectrochemical analytical studies

Photoelectrochemical measurements were performed with a conventional 3-electrode cell connected to a Metrohm Autolab PGSTAT 204 potentiostat. The working electrodes FTO/Ti Fe_2O_3/"Ni" are described in paragraphs 2.1 and 2.2. The counter electrode is a platinum wire. The reference electrode is an Ag/AgCl electrode. All electrolyte solutions are prepared from analytical grade NaOH (VWR, 98.6%) and urea (VWR, 99.8%).

The electrolyte is an aqueous solution of NaOH at 1 mol L^{-1} (pH = 13.6), with or without urea at 0.33 mol L^{-1}. Voltammetric curves were established at 10 mV s^{-1}. They are presented with the potentials given according to the reversible hydrogen electrode (RHE), after conversion according to:

$$E\ (V\ vs.\ RHE) = E\ (V\ vs.\ Ag/AgCl) + 0.208 + 0.059\ pH$$

The measurements under illumination were performed using a Newport LSH7320 solar simulator delivering AM 1.5G light with a power of 1000 W m^{-2}.

2.6 Photoelectrolysis

The photoelectrochemical device used for photoelectrolysis is described in Figure S5 in SI.

Gas chromatography. To collect the gases produced during the photoelectrooxidation of urea and water (N_2 and O_2, respectively), an *in situ* gas collection device in the anode compartment has been set up, which is directly connected to the gas chromatograph to avoid contamination by air (see Figure S5). A MicroGas CP-4900 chromatograph from Varian was used, equipped with a 5Å CP-Molsieve column (10 m) under argon and a moisture filter.

Ionic chromatography. A Dionex ICS-5000+ System chromatograph (Thermo Scientific) was employed with IonPac TM AS19 4 µm (2 x 250 mm, 0.25 mL min^{-1}) and IonPac CS16 4 µm (5 x 500 mm, 1 mL min^{-1}) columns for anions and cations, respectively. High purity hydroxide eluents for gradient runs were obtained using an electrolytic eluent generator and methanesulfonic acid (30 mM) eluent for isocratic runs were prepared manually.

Urea determination. Urea removal rates were determined by optical absorption using Megazymes enzyme assay kits and a Hitachi U-41000 spectrometer.

2.7 *In situ* spectrophotometric measurements

A silicon photodiode (Hamamatsu) placed behind the photoelectrode and the photoelectrochemical cell (see diagram in Figure S6 in SI) is used to measure a photocurrent proportional to the transmittance, which is recorded by the potentiostat simultaneously with the cyclic voltammetry. The spectral range of silicon extends significantly beyond that of hematite (1100 nm vs. 590 nm). The photodiode signal, therefore, corresponds mainly to photons with wavelengths between 590 nm and 1100 nm, with a variation of about 10% depending on the state of the nickel in the deposited layer, *i.e.* $Ni(OH)_2$ or NiOOH.

3. Results and discussion

3.1 Morphology and optical properties of photoanodes FTO/Ti-Fe_2O_3/Ni

Plane view and cross-section images of FTO/Ti-Fe_2O_3 samples are shown in Figure 1, before (A) and after Ni deposition by sputtering (2 nm, B) and NiOOH PEC deposition (17.5 mC cm^{-2}, C), followed by electrochemical cycling in NaOH 1 mol L^{-1}.

The hematite film on the surface of the FTO layer appears as agglomerates of nanorods with an average height of ~ 400 nm and width of ~ 150 nm (Figure 1A). These agglomerates are spaced by 50-100 nm wide trenches, at which the FTO substrate can be observed (circle and red arrow).

The visible roughness at the top of the nanorods corresponds to the deposition of Ni (Figure 1B-C). In the plan view, we see that they are sheets oriented perpendicularly to the surface, typical of $Ni(OH)_2$/NiOOH. In the case of sputtering deposition (Figure 1B), Ni is sometimes present down to the base of nanorods, which is made possible by the presence of trenches. It is therefore likely that Ni is also deposited on the FTO layer in these areas. In the case of NiOOH deposition by PED, the cross-section (Figure 1C) shows that Ni_{PEC} is found only at the top of the nanorods, with a clear stop at mid-height (see Figure S7 in SI for a lower magnification view).

Figure 2 shows the absorptance of FTO/Ti-Fe_2O_3 samples before and after Ni coverage by sputtering (2 nm, A) and by PEC deposition (8.75 mC cm^{-2}, B).

The sputtering deposition of 2 nm Ni results in almost identical optical properties to the initial Ti-Fe_2O_3 layer on the useful part of the spectrum for hematite (350-590 nm). In the case of PEC deposition, a slight decrease in absorptance at short wavelengths is observed which is due to a higher reflectivity.

The fact that the absorptance remains important (from 55 to 30%) at wavelengths above 590 nm is related to the combination of several factors: the existence of electronic transitions in Ti-Fe_2O_3 corresponding to an indirect bandgap of 1.9 eV, the existence of states in its bandgap related to surface defects [25] and the absorption by free carriers of the highly doped FTO layer (F-SnO_2).

From these spectra, the maximum photocurrent densities achievable under AM1.5G solar illumination (*i.e.*, with QE = 1 between 350 and 590 nm), are theoretically 10.7 and 10.8 mA cm^{-2} for the samples with sputtered Ni and PEC deposited NiOOH, respectively. This is lower than the theoretical maximum photocurrent of 12.5 mA cm^{-2} for Fe_2O_3, mainly because of reflection losses.

3.2 Photoelectrochemical properties of FTO/Ti-Fe_2O_3/Ni

3.2.1 Sputtered Ni

Voltammograms of a Ti-Fe_2O_3 photoelectrode measured in the dark and under solar illumination in a 1 mol L^{-1} NaOH solution (dashed and solid blue curves, respectively) are presented in Figure 3A.

In the dark, Ti-Fe_2O_3 gives no anodic current up to 1.75 V_{RHE} (blue dashed curve), in agreement with the absence of $h+$ as majority carriers in n-type hematite. The increase in current from 1.75 V_{RHE} is attributed to the oxidation of water on FTO.

After depositing Ni_{SP} (2 nm), a couple of anodic and cathodic peaks are observed in the dark at 1.48 and 1.33 V_{RHE} (red dashed curve) which corresponds to the $Ni^{II}(OH)_2/Ni^{III}OOH$ system. These signals are stable after the five cycles required for the development of these species on the surface (see Figure S2 in SI). Considering the blocking character of n-type Ti-Fe_2O_3 and the potential of the peaks, these signals correspond to Ni deposited on FTO areas between the Ti-Fe_2O_3 nanorods (*cf.* circle and red arrow of Figure 1A, and EDX analysis Figure S8 in SI).

Under illumination, the photocurrent for water oxidation on Ti-Fe_2O_3 starts at 0.95 V_{RHE}, with a pseudo-plateau from 1.30 V_{RHE} and beyond. The addition of Ni (red curve) does not lead to any gain in the photocurrent onset potential, whereas NiOOH normally plays the role of catalyst for water oxidation, as it has been previously reported in electrochemistry [26] or photoelectrochemistry, especially on Fe_2O_3 [20]. There is though a small oxidation/reduction signal at the onset of

photocurrent. Moreover, we note that the signal from the $Ni(OH)_2$/NiOOH couple present in the dark (FTO/Ni_{SP}) adds to the photocurrent. More importantly, the addition of Ni_{SP} results in a decrease of the photocurrent by a factor of 2, despite the assumed catalytic effect of NiOOH already mentioned.

The photocurrent values determined at 1.23 V_{RHE} and 1.40 V_{RHE} (*i.e.* before the Ni signal on FTO) are reported in the table of Figure 3.

Figure 3B allows to observe the effect of urea on the response of Ti-Fe_2O_3/Ni_{SP}. In the dark and in presence of urea, the anodic current increases very strongly from 1.35 V_{RHE} due to the oxidation of urea at FTO/Ni_{SP} areas. Under illumination, the photocurrent appears at a potential ~ 100 mV more negative with urea than in NaOH and is ~ 50% more intense at 1.23 V_{RHE}. From the table of Figure 3, we notice that the photocurrent is always lower than that obtained for Ti-Fe_2O_3 without Ni (0.35 *vs.* 0.45 mA cm^{-2} at 1.23 V_{RHE}), despite the expected catalytic effect of Ni on urea oxidation [20].

3.2.2 Photoelectrodeposited NiOOH

Figure 4A shows voltammograms of a Ti-Fe_2O_3 sample before and after NiOOH PEC deposition (8.75 mC cm^{-2}, Ni_{PEC}) in NaOH (A) and NaOH + urea (B), respectively.

The voltammograms of Ti-Fe_2O_3 in NaOH measured in the dark and under illumination are similar to those described for sputtered Ni (Figure 3A). After depositing NiOOH, Ti-Fe_2O_3/Ni_{PEC} appears to block current in the dark, without any parasitic peaks from FTO/Ni. Under illumination, the $Ni(OH)_2$/NiOOH peaks are centered at 0.90 V_{RHE}. This potential is much lower than that for a conventional Ni electrode (1.40 V_{RHE}), *i.e.*, it represents a potential gain of 0.5 V. The presence of Ni_{PEC} results in a photocurrent onset potential shift of -50 mV compared to Ti-Fe_2O_3 (Figure 4A), with a ~10% higher photocurrent pseudo-plateau (values listed in the table of Figure 4).

In NaOH + urea and in the dark (Figure 4B), a small peak appears at 1.55 V_{RHE}, probably related to a very small amount of Ni deposited on FTO, of which the signal in NaOH is even not distinguishable.

Under illumination, the photocurrent starts from the $Ni(OH)_2$ oxidation peak (0.7 V_{RHE}) and is higher than the photocurrent measured in the presence of NaOH only (Figure 4A). This could suggest that at least 10-20% of the photocurrent is related to urea oxidation.

Figure 4C compares the voltammograms of the two types of Ni deposition under the conditions expected for the application, *i.e.*, NaOH 1 mol L^{-1} with 0.33 mol L^{-1} of urea (similar to that in urine). The PEC deposition appears to be more efficient than the sputtering deposition, with (i) the absence of parasitic peaks due to the selectivity of deposition on Ti-Fe_2O_3, (ii) active Ni sites twice more important, and finally beneficial potential shift on the photoelectrochemical response by -200 mV.

3.2.3 *In situ* transmittance measurements

Cyclic voltammetry cannot provide more information about the catalytic mechanisms involved in the oxidation of water and urea at the active Ni sites. The electrochromic properties of $Ni(OH)_2$/NiOOH are already well known [27,28] and the fact that NiOOH absorbs visible light, while $Ni(OH)_2$ is transparent, offers the possibility to evaluate the proportions of these two forms during

photoelectrocatalysis by considering that the transmittance depends on the surface concentration of NiOOH according to the Beer-Lambert-Bouguer law. *In situ* transmittance measurements were performed during cyclic voltammetry under different urea concentrations for samples with Ni deposited either by sputtering or by PED.

Sputtered Ni. Figure 5 shows voltammograms and transmittance measurements obtained with Ti-Fe_2O_3/Ni_{SP} (A and B, respectively). The transmittance is normalized to 1 at the equilibrium potential, ~ 0.8 V_{RHE}, *i.e.*, when $Ni(OH)_2$ (transparent) is predominant.

In the absence of urea and when the photoelectrode is swept anodically (red curve), $Ni(OH)_2$ is converted to NiOOH with consequently a transmittance that decreases and tends to a minimum value (red curve, 1.8 V_{RHE}). This evolution is marked by two successive drops, one starting at 0.85 V_{RHE}, the other at 1.40 V_{RHE}. Comparing with the voltammograms of Figure 5A, the first one must correspond to Ni_{SP} deposited on Ti-Fe_2O_3 nanorods, the second one to Ni_{SP} deposited on FTO.

On the reverse sweep (*i.e.*, to cathodic potentials), the transmittance describes a quasi-plateau, then increases due to the reduction of NiOOH to $Ni(OH)_2$, first on FTO, then on Ti-Fe_2O_3.

When urea is added at 10, 50, 100, 150, and 300 mmol L^{-1}, the minimum in transmittance, measured at ~1.85 V_{RHE}, increases relative to NaOH alone, in proportion to the urea concentration. The transmittance corresponding specifically to Ti-Fe_2O_3/Ni_{SP} (not FTO/Ni_{SP}) is highlighted in Figure 5B by a dashed line at 1.27 V_{RHE}.

The increase in transmittance reveals a decrease in the number of NiOOH sites, which agrees with an EC process (Electrochemical reaction followed by a Chemical reaction). Indeed, if the mechanism was direct (electrochemical oxidation of urea on NiOOH), there would be no influence of the urea concentration on the transmittance. This EC mechanism was proposed by Vedharathinam and Botte based on Raman spectroscopy studies [29]. It is directly confirmed by these UV-Vis *in situ* transmittance measurements and for the first time in a photoelectrochemical process.

PEC deposited NiOOH. Figure 6 shows the voltammograms and transmittance measurements obtained with Ti-Fe_2O_3/Ni_{PEC} (A and B, respectively).

In the absence of urea, the transmittance starts to drop at ~ 0.75 V_{RHE}, which corresponds to the onset of photocurrent. Contrary to the sputtering case, only one step is observed since photoelectrodeposition takes place almost exclusively on Ti-Fe_2O_3 nanorods. The sharp increase in photocurrent from 1.60 V_{RHE} is not associated with a change of transmittance since it corresponds to the oxidation of water.

The backward scan gives a stable transmittance plateau for which 100% of the active Ni sites are in the NiOOH state. The dashed line at 1.27 V_{RHE} is used to compare the transmittance value with that obtained for sputtered Ni (0 mmol L^{-1}, Figure 5B). The decrease in transmittance with Ni_{PEC} is 8.6% (a. v.) *vs.* 4.1% (a. v.) with Ni_{SP}. This means that there are twice as many active NiOOH sites at this potential with PEC deposition.

This result is confirmed by a deposition study performed directly on bare FTO. From voltammograms recorded in 1 mol L^{-1} NaOH (Figure S9), the amount of active Ni sites, calculated from the oxidation peak of $Ni(OH)_2$ to NiOOH, is 1.65 times higher by PEC deposition than by sputtering (28 nanomoles cm^{-2} for a PEC deposition of 8.75 mC cm^{-2} and 17 nanomoles cm^{-2} for a sputtering deposit of 2 nm).

Between 0 and 50 mmol L^{-1} of urea, the maximum transmittance (at 1.27 V_{RHE}) varies linearly with the concentration. Kinetics are mainly controlled by the diffusion of urea to the surface. From 50 to 300 mmol L^{-1}, the decrease in transmittance saturates, implying that it is the catalytic process that limits the kinetics. It may be assumed that the sites are blocked in the reduced $Ni(OH)_2$ state for some time due to adsorbed reaction intermediates preventing their oxidation to NiOOH. At 300 mmol L^{-1} of urea, the decrease in transmittance is three times smaller than without urea (-3.0 % vs. -8.6 %, respectively). If we assume that all active Ni sites are engaged in a catalytic cycle between the two states, it implies that at any moment there is about 1/3 of the active sites that are in the NiOOH state, meaning that the rate of electrochemical oxidation is twice as small as the rate of chemical reduction by urea.

3.2.4 Discussion

The results of photoelectrochemistry and *in situ* transmittance measurements show a significant difference between the two methods of Ni deposition.

The oxidation/reduction peaks of the $Ni(OH)_2$/NiOOH are shifted in both cases from 1.40 to 0.9 V_{RHE} under illumination, due to the h^+ photogenerated in the valence band of Ti-Fe_2O_3, *i.e.*, at more positive potentials than the potential of the electrode. They are however hardly visible in the Ni-sputtering case, and on the contrary very apparent in the NiOOH PEC deposition method. Such a shift has already been reported for the electrochemical deposition of NiOOH on hematite [30], or the ALD deposition of NiO on hematite [31] in studies on solar water splitting (OER).

Other methods of Ni deposition on hematite have been used in urea oxidation studies, such as dip coating [9,12] or cathodic electrodeposition [10]. However, a comparison with the present study regarding the position of $Ni(OH)_2$/NiOOH peaks is not possible because voltammograms in NaOH without urea, on which these peaks are visible, are not reported.

In the case of sputtering, a strong decrease of the photocurrent in NaOH is observed after deposition. The *in-situ* transmittance measurements show that it is not due to a decrease in the light transmitted through the Ni layer. For example, at 1.27 V_{RHE} in NaOH, the photocurrent drops by 50% (see Figure 3A) while the transmittance decreases by only 4% (see Figure 5B). This is confirmed by the measurement of the specific absorption spectrum of a NiOOH film formed under anodic polarization in NaOH (see Figure S10 in SI), which is found to be between 5% at 590 nm and 10% at 400 nm.

The most likely explanation is that sputtering creates defects at the Ti-Fe_2O_3/Ni_{SP} interface that led to significant recombination of photogenerated h^+ in Ti-Fe_2O_3, as is often observed for sputtered metals on semiconductors.

In the case of PEC deposited Ni, photoelectrooxidation of water on Ti-Fe_2O_3/Ni_{PEC} appears to begin as early as 0.68 V_{RHE} *vs.* 0.85 V_{RHE} on bulk Ti-Fe_2O_3. However, Young and Hamann, who obtained the same type of results with NiO deposits, were able to show by current transient measurements that the peak corresponds to the oxidation of $Ni(OH)_2$ only, not to the HER [31]. In our case, we similarly observe that the photocurrent at the oxidation peak of $Ni(OH)_2$ in NaOH (*i.e.*, between 0.7 and 0.9 V_{RHE}) is not amplified upon addition of urea (Figure 4B). therefore, urea oxidation really starts at 0.9 V_{RHE}, which is consistent with the fact that the decrease in transmittance is affected by urea addition only above 0.9 V_{RHE} (Figure 6B).

On Ni electrodes, it is typical to obtain a current amplification factor of ~8 between the urea oxidation peak (at 0.3 mol L^{-1}) and the $Ni(OH)_2$ oxidation peak [32]. In the case of FTO/Ti-Fe_2O_3/Ni_{PEC} under solar illumination, the amplification factor of the photocurrent (pseudo-plateau) reaches ~1.2 at best. This discrepancy shows that the system is mainly limited by the collection of photogenerated h^+ charges in hematite and/or by their recombination at the interface.

3.3 Urea electrolysis

To determine the faradaic efficiencies of the competing water and urea photoelectrooxidation reactions, we performed quantitative photoelectrolysis of urea on FTO/ Ti-Fe_2O_3/Ni_{PEC} electrodes.

Firstly, urea was determined before and after electrolysis to calculate the abatement rate. To obtain significant concentration differences, the starting solution (1 mol L^{-1} of NaOH) contained 0.012 mol L^{-1} of urea which is 30 times lower than the classical concentration of urea in urine (~0.3 mol L^{-1}). Two photoelectrolysis were conducted with a Ti-Fe_2O_3/Ni_{PEC} photoelectrode (8.75 mC cm^{-2}) at 1.51 V_{RHE} for 6 hours under AM1.5G (constant temperature of 23°C). Abatement rates of 40 and 38 ± 7% were measured, demonstrating the activity of photoelectrodes towards in urea oxidation. No decrease in urea concentration was observed in a control experiment at zero current under the same illumination conditions (6 hours under 1000 W m^{-2}, AM1.5G, 23°C), indicating that urea does not spontaneously decompose under prolonged solar illumination (in NaOH 1 mol L^{-1}).

Secondly, to quantify the reaction products, four electrolysis were conducted with FTO/Ti-Fe_2O_3/Ni_{PEC} photoelectrodes (8.75 mC cm^{-2}) under solar illumination for 4 h in a solution of 1 mol L^{-1} NaOH and 0.33 mol L^{-1} urea. The applied potential was 1.51 V_{RHE}, which corresponds to the photocurrent pseudo-plateau (see Figure 6A). The GC revealed the presence of N_2 and O_2 as well as traces of H_2. For one of the electrolysis, the solution was also analyzed by ion chromatography (IC). The IC showed the presence of NO_2^- (and traces of cyanates (CNO^-) already present in the initial

solution). The faradaic efficiency for each product (N_2, O_2, NO_2^-) was calculated from the quantities formed. The results are given in Table 1.

Table 1. Faradaic yields of products formed in the gas and liquid phase during four photoelectrolysis with FTO/Ti-Fe_2O_3/Ni_{PEC} of a 0.33 mol L^{-1} urea solution in 1 mol L^{-1} NaOH at 1.51 V_{RHE} during 4 h.

electrolysis		O_2		N_2		NO_2^-		Σ (calculated charges) /Total charge (%)
	Total charge (C)	calculated charge (C)	yield (%)	calculated charge (C)	yield (%)	calculated charge (C)	yield (%)	
E1	23.2	3.1	13.3	2.3	10.0	/	/	23.2
E2	25.3	8.9	35.0	2.8	11.1	/	/	46.3
E3	25.0	2.3	9.3	4.4	17.6	/	/	26.8
E4	**27.2**	**4.0**	**14.8**	**4.7**	**17.3**	**17.4**	**64.9**	**96.0**
Average	25.2 ± 2	4.6 ± 4	18.1 ± 12	3.6 ± 1	14.0 ± 4	/	/	/

It is observed that the yield of N_2 formation is relatively low, reaching at best 17.6 %. At the same time, the evolution of O_2 is not negligible, with a yield varying between 9 and 35 %. In total, the formation of these two species represents only 23 to 46 % of the charge transferred. In the case of electrolysis E4 where the ionic species formed in solution were measured, most of this charge is related to the formation of nitrites (65%). N_2, O_2 and nitrites account for 96% of the past charge. This is in good agreement with results obtained for conventional electrocatalysis of urea solutions on Ni plates, where the faradaic efficiency for nitrite is measured at ~60% (unpublished results). Recently, Li *et al.* have reported for the first time the formation of nitrites during urea electrolysis on Ni foam electrodes with faradaic efficiencies up to 80% [33].

Eventually, it appears that ~80% of the charges are involved in the oxidation of urea (to N_2 and NO_2^-), a conclusion that could not be drawn from the comparison between voltammograms measured in NaOH and in urea (Figure 4B).

Based on these results, which are reported for the first time in terms of the balance of electrolysis products formed by photoelectrooxidation of urea, we demonstrate that photoelectrocatalysis of urea on hematite with a nickel ($Ni(OH)_2$/NiOOH) catalyst can effectively oxidize urea to N_2. The yield is modest (10-18%) but it is a starting point without any particular optimization of the photoelectrolysis conditions (applied potential, stirring, etc.). From the point of view of a pollution control application where the aim is to remove nitrogen (in particular in the form of an inert gas like N_2) before treatment in a WWTP, the important part of nitrite formed, a soluble product which remains in solution, is a problem which requires a strong improvement of the selectivity, either by finding more favorable electrolysis conditions (*e.g.*, adjustment of the potential, pulsed electrolysis), or by modifying the catalyst (*e.g.*, increasing the active surface, adding a co-element to Ni). The interest of the Ti-Fe_2O_3/Ni_{PEC} photoelectrodes developed in this work lies in the -500 mV gain in potential under solar illumination that they allow compared to a metallic Ni electrode.

4. Conclusion

The performances of FTO/Ti-Fe_2O_3 photoelectrodes decorated with sputter-deposited Ni or photoelectrodeposited NiOOH towards the photoelectrooxidation of urea under solar illumination has been studied. For thickness optimized deposition, it appears that PEC deposition is more efficient than sputtering deposition. The latter suffers from recombination at the interface (photocurrent reduced by a factor of 2) and by a lower number of active Ni sites, as *in situ* transmittance measurements have shown. Ni PEC deposited on FTO/Ti-Fe_2O_3 gives a couple of $Ni(OH)_2$/NiOOH peaks centered at 0.90 V_{RHE}, a potential gain of 0.50 V compared to a conventional Ni metal electrode under the same conditions (1.40 V_{RHE}).

In situ transmission measurements confirmed that the mechanism of urea oxidation is EC. At 300 mmol L^{-1} urea under 1.27 V_{RHE}, it appears that 2/3 of the Ni sites are in the $Ni(OH)_2$ state and 1/3 in the NiOOH state, *i.e.*, the lifetime of $Ni(OH)_2$ is twice longer than NiOOH. This technique will be developed to access kinetic and catalytic constants.

Quantitative photoelectrolysis was carried out and gave faradaic efficiencies ranging from 10 to 18% for N_2 and 9 to 35% for O_2. The remaining passed charges are involved in significant nitrite production (~ 65%), which points to the existence of another reaction pathway than the one leading to N_2 (R1). In the end, photoelectrooxidation of urea accounts for ~ 80% of the passed charge. These results clearly demonstrate the feasibility of removing nitrogen from urea in solution as N_2 in air by a photoelectrocatalytic process using FTO/Ti-Fe_2O_3/Ni photoelectrodes under solar illumination. However, significant progress is still needed, especially to improve its selectivity towards N_2 production and its overall photovoltaic conversion efficiency.

CRediT authorship contribution statement

L. Rebiai : Experiments, Investigation, Validation, Data curation, Writing – review & editing, Visualization, **D. Muller-Bouvet:** Investigation, Data curation, **R. Benyahia:** Investigation, Validation, Data curation, **E. Torralba:** Resources, **C. Cachet-Vivier:** Conceptualization, Writing – original draft, Writing – review & editing, Supervision, Project administration, Funding acquisition, **Melissa Lopez Viveros :** Conceptualization, Writing – review & editing, **Vincent Rocher :** Conceptualization, Writing – review & editing, **Sam Azimi:** Conceptualization, Writing – review & editing, **S. Bastide:** Conceptualization, Methodology, Writing – review & editing, Visualization, Supervision, Funding acquisition.

Declaration of Competing Interest

The authors declare that they have no known competing financial interests or personal relationships that could have appeared to influence the work reported in this paper.

Acknowledgements

This work is supported by the French National Research Agency in the framework of the HYUREA project (19-CE04-0009). L. Rebiai acknowledges the Doctoral School "Science, Ingénierie et Environnement" at Paris Est Sup for her PhD Research Fellowship and R. Pires for the scanning electron microscopy training. The authors also thank L. Latapie for the IC analyses conducted at the Chemical Engineering Laboratory (LGC) of Toulouse.

Supplementary material

PDF file containing "Supplementary Information".

References

[1] Y. Gu, Y. Li, X. Li, P. Luo, H. Wang, X. Wang, J. Wu, F. Li, Energy Self-sufficient Wastewater Treatment Plants: Feasibilities and Challenges, Energy Procedia. 105 (2017) 3741–3751. https://doi.org/10.1016/j.egypro.2017.03.868.

[2] S. Azimi, V. Rocher, Energy consumption reduction in a wastewater treatment plant, Water Practice and Technology. 12 (2017) 104–116. https://doi.org/10.2166/wpt.2017.006.

[3] W. Xu, Z. Wu, S. Tao, Urea-Based Fuel Cells and Electrocatalysts for Urea Oxidation, Energy Technol. 4 (2016) 1329–1337. https://doi.org/10.1002/ente.201600185.

[4] K. Ye, G. Wang, D. Cao, G. Wang, Recent Advances in the Electro-Oxidation of Urea for Direct Urea Fuel Cell and Urea Electrolysis, Top Curr Chem (Z). 376 (2018) 42. https://doi.org/10.1007/s41061-018-0219-y.

[5] E. Urbanczyk, M. Sowa, W. Simka, Urea removal from aqueous solutions-a review, J. Appl. Electrochem. 46 (2016) 1011–1029. https://doi.org/10.1007/s10800-016-0993-6.

[6] X. Sun, R. Ding, Recent progress with electrocatalysts for urea electrolysis in alkaline media for energy-saving hydrogen production, Catal. Sci. Technol. 10 (2020) 1567–1581. https://doi.org/10.1039/C9CY02618E.

[7] B.K. Boggs, R.L. King, G.G. Botte, Urea electrolysis: direct hydrogen production from urine, Chem. Commun. (2009) 4859–4861. https://doi.org/10.1039/B905974A.

[8] B. Zhu, Z. Liang, R. Zou, Designing Advanced Catalysts for Energy Conversion Based on Urea Oxidation Reaction, Small. 16 (2020) 1906133. https://doi.org/10.1002/smll.201906133.

[9] G. Wang, Y. Ling, X. Lu, H. Wang, F. Qian, Y. Tong, Y. Li, Solar driven hydrogen releasing from urea and human urine, Energy Environ. Sci. 5 (2012) 8215–8219. https://doi.org/10.1039/C2EE22087C.

[10] D. Xu, Z. Fu, D. Wang, Y. Lin, Y. Sun, D. Meng, T. feng Xie, A $Ni(OH)_2$-modified Ti-doped α-Fe_2O_3 photoanode for improved photoelectrochemical oxidation of urea: the role of $Ni(OH)_2$ as a cocatalyst, Phys. Chem. Chem. Phys. 17 (2015) 23924–23930. https://doi.org/10.1039/C5CP03310A.

[11] W.M. Omymen, J.R. Rogan, B.Z. Jugović, M.M. Gvozdenović, B.N. Grgur, Photo-assisted electrochemical oxidation of the urea onto TiO_2-nanotubes modified by hematite, Journal of Saudi Chemical Society. 21 (2017) 990–997. https://doi.org/10.1016/j.jscs.2017.05.010.

[12] J. Gan, B.B. Rajeeva, Z. Wu, D. Penley, Y. Zheng, Plasmon-enhanced hierarchical photoelectrodes with mechanical flexibility for hydrogen generation from urea solution and human urine, J Appl Electrochem. 50 (2020) 63–69. https://doi.org/10.1007/s10800-019-01369-0.

[13] Gurudayal, P.S. Bassi, T. Sritharan, L.H. Wong, Recent progress in iron oxide based photoanodes for solar water splitting, J. Phys. D: Appl. Phys. 51 (2018) 473002. https://doi.org/10.1088/1361-6463/aae138.

[14] T. Lindgren, H. Wang, N. Beermann, L. Vayssieres, A. Hagfeldt, S.-E. Lindquist, Aqueous photoelectrochemistry of hematite nanorod array, Solar Energy Materials and Solar Cells. 71 (2002) 231–243. https://doi.org/10.1016/S0927-0248(01)00062-9.
[15] A.G. Tamirat, J. Rick, A.A. Dubale, W.-N. Su, B.-J. Hwang, Using hematite for photoelectrochemical water splitting: a review of current progress and challenges, Nanoscale Horiz. (2016). https://doi.org/10.1039/C5NH00098J.
[16] A. Tofanello, S. Shen, F.L. de Souza, L. Vayssieres, Strategies to improve the photoelectrochemical performance of hematite nanorod-based photoanodes, APL Materials. 8 (2020) 040905. https://doi.org/10.1063/5.0003146.
[17] E. López-Fernández, J. Gil-Rostra, J.P. Espinós, A.R. González-Elipe, A. de Lucas Consuegra, F. Yubero, Chemistry and Electrocatalytic Activity of Nanostructured Nickel Electrodes for Water Electrolysis, ACS Catal. 10 (2020) 6159–6170. https://doi.org/10.1021/acscatal.0c00856.
[18] S. Corby, M.-G. Tecedor, S. Tengeler, C. Steinert, B. Moss, C.A. Mesa, H.F. Heiba, A.A. Wilson, B. Kaiser, W. Jaegermann, L. Francàs, S. Gimenez, J.R. Durrant, Separating bulk and surface processes in NiO_x electrocatalysts for water oxidation, Sustainable Energy Fuels. 4 (2020) 5024–5030. https://doi.org/10.1039/D0SE00977F.
[19] P. Qiu, F. Li, H. Zhang, S. Wang, Z. Jiang, Y. Chen, Photoelectrochemical performance of α-Fe_2O_3@NiOOH fabricated with facile photo-assisted electrodeposition method, Electrochimica Acta. 358 (2020) 136847. https://doi.org/10.1016/j.electacta.2020.136847.
[20] F. Malara, A. Minguzzi, M. Marelli, S. Morandi, R. Psaro, V. Dal Santo, A. Naldoni, α-Fe_2O_3/NiOOH: An Effective Heterostructure for Photoelectrochemical Water Oxidation, ACS Catal. 5 (2015) 5292–5300. https://doi.org/10.1021/acscatal.5b01045.
[21] A.G. Tamirat, W.-N. Su, A.A. Dubale, H.-M. Chen, B.-J. Hwang, Photoelectrochemical water splitting at low applied potential using a NiOOH coated codoped (Sn, Zr) α-Fe_2O_3 photoanode, J. Mater. Chem. A. 3 (2015) 5949–5961. https://doi.org/10.1039/C4TA06915C.
[22] D.A. Daramola, D. Singh, G.G. Botte, Dissociation Rates of Urea in the Presence of NiOOH Catalyst: A DFT Analysis, J. Phys. Chem. A. 114 (2010) 11513–11521. https://doi.org/10.1021/jp105159t.
[23] Y.-J. Chen, L.-Y. Chen, The study of carrier transfer mechanism for nanostructural hematite photoanode for solar water splitting, Applied Energy. 164 (2016) 924–933. https://doi.org/10.1016/j.apenergy.2015.08.105.
[24] C. Natarajan, H. Matsumoto, G. Nogami, Improvement in Electrochromic Stability of Electrodeposited Nickel Hydroxide Thin Film, J. Electrochem. Soc. 144 (1997) 121. https://doi.org/10.1149/1.1837373.
[25] C. Du, M. Zhang, J.-W. Jang, Y. Liu, G.-Y. Liu, D. Wang, Observation and Alteration of Surface States of Hematite Photoelectrodes, J. Phys. Chem. C. 118 (2014) 17054–17059. https://doi.org/10.1021/jp5006346.
[26] M.S. Burke, S. Zou, L.J. Enman, J.E. Kellon, C.A. Gabor, E. Pledger, S.W. Boettcher, Revised Oxygen Evolution Reaction Activity Trends for First-Row Transition-Metal (Oxy)hydroxides in Alkaline Media, J. Phys. Chem. Lett. 6 (2015) 3737–3742. https://doi.org/10.1021/acs.jpclett.5b01650.
[27] J. Velevska, M.P. Gjorgjevich, N. Stojanov, Electrochromic Nickel Oxide Thin Films for Solar Light Modulation, International Journal of Sciences: Basic and Applied Research. 31 (2017) 94–104. https://gssrr.org/index.php/JournalOfBasicAndApplied/article/view/6856.
[28] H. Nolan, M.P. Browne, N.C. Berner, G.S. Duesberg, P.E. Colavita, M.E.G. Lyons, Electrochromic Nickel Oxide Films for Smart Window Applications, Int. J. Electrochem. Sci. 11 (2016) 6636–6647. https://doi.org/10.20964/2016.08.38.
[29] V. Vedharathinam, G.G. Botte, Direct evidence of the mechanism for the electro-oxidation of urea on Ni(OH)2 catalyst in alkaline medium, Electrochimica Acta. 108 (2013) 660–665. https://doi.org/10.1016/j.electacta.2013.06.137.
[30] C.G. Morales-Guio, M.T. Mayer, A. Yella, S.D. Tilley, M. Grätzel, X. Hu, An Optically Transparent Iron Nickel Oxide Catalyst for Solar Water Splitting, Journal of the American Chemical Society. 137 (2015) 9927–9936. https://doi.org/10.1021/jacs.5b05544.

[31] K.M.H. Young, T.W. Hamann, Enhanced photocatalytic water oxidation efficiency with $Ni(OH)_2$ catalysts deposited on α-Fe_2O_3 via ALD, Chem. Commun. 50 (2014) 8727–8730. https://doi.org/10.1039/C4CC02598A.
[32] A.T. Miller, B.L. Hassler, G.G. Botte, Rhodium electrodeposition on nickel electrodes used for urea electrolysis, J Appl Electrochem. 42 (2012) 925–934. https://doi.org/10.1007/s10800-012-0478-1.
[33] J. Li, J. Li, T. Liu, L. Chen, Y. Li, H. Wang, X. Chen, M. Gong, Z. Liu, X. Yang, Deciphering and Suppressing Over- Oxidized Nitrogen in Nickel- Catalyzed Urea Electrolysis, Angew. Chem. Int. Ed. 60 (2021) 26656–26662. https://doi.org/10.1002/anie.202107886.

Photoelectrocatalytic conversion of urea under solar illumination using Ni decorated Ti-Fe_2O_3 electrodes

Lamia Rebiai *et al.*

Graphical Abstract

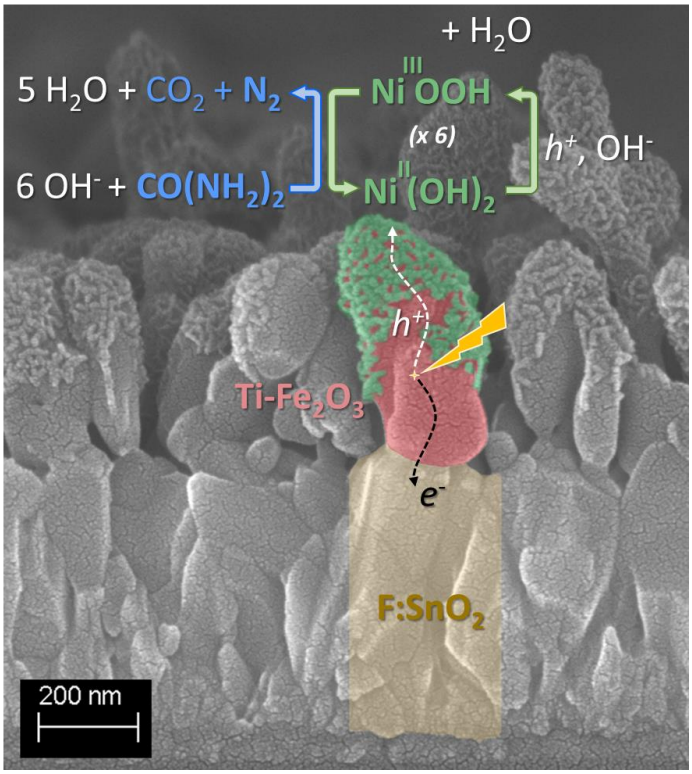

Photoelectrocatalytic conversion of urea under solar illumination using Ni decorated Ti-Fe_2O_3 electrodes

Lamia Rebiai *et al.*

FIGURES

Figure 1. SEM plane view and cross-section images of Ti-Fe_2O_3 samples before (A) and after deposition of 2 nm of Ni by sputtering (B) or after NiOOH PEC deposition at 17.5 mC cm^{-2} (C). Scale bars: 100 and 200 nm for plan view and cross-section images, respectively. For cross-section imaging, metallization with 2 nm of $Pt_{80}Pd_{20}$ was applied to avoid charge accumulation.

Figure 2. Absorptance and reflectance of FTO/Ti-Fe_2O_3 samples, with or without sputtered Ni (2 nm, A) and PEC deposited Ni (8.75 mC cm^{-2}, B). The dashed line at 590 nm corresponds to the gap of Fe_2O_3 (2.1 eV).

Figure 3. Voltammetry in the dark and under illumination of (A) FTO/Ti-Fe_2O_3 in NaOH, before and after sputtering deposition of 2 nm of Ni (Ti-Fe_2O_3/Ni_{sp}); (B) Ti-Fe_2O_3/Ni_{sp} in NaOH with or without urea. Table: Photocurrent values of both FTO/Ti-Fe_2O_3 and Ti-Fe_2O_3/Ni_{SP} electrodes at 1.23 et 1.40 V_{RHE}. [NaOH] = 1 mol L^{-1}; [urea] = 0.33 mol L^{-1}. Scan rate: 10 mV s^{-1}. Illumination: AM1.5G, 1000 W m^{-2}.

Figure 4. Voltammetry in the dark and under illumination of (A) FTO/Ti-Fe_2O_3 in NaOH, before and after PEC deposition of NiOOH (8.75 mC cm^{-2}); (B) Ti-Fe_2O_3/Ni_{PEC} in NaOH, with or without urea; (C) FTO/Ti-Fe_2O_3/Ni_{SP} and FTO/Ti-Fe_2O_3/Ni_{PEC} in NaOH with urea (under illumination only). Table: Photocurrent values of both FTO/Ti-Fe_2O_3 and Ti-Fe_2O_3/Ni_{PEC} electrodes at 1.23 et 1.50 V_{RHE}. [NaOH] = 1 mol L^{-1}; [urea] = 0.33 mol L^{-1}. Scan rate: 10 mV s^{-1}. Illumination: AM1.5G, 1000 W m^{-2}.

Figure 5. (A) Voltammetry under illumination of FTO/Ti-Fe_2O_3/Ni_{SP} (2 nm) in NaOH and different concentrations of urea, with an insert showing the photocurrent onset potential region; (B) Transmittance measured *in situ* during voltammetry. [NaOH] = 1 mol L^{-1}; [urea] = 0, 10, 50, 150 and 300 mmol L^{-1}. Scan rate: 2 mV s^{-1}. Illumination: AM1.5G, 1000 W m^{-2}.

Figure 6. (A) Voltammetry under illumination of FTO/Ti-Fe_2O_3/Ni_{PEC} (8.75 mC cm^{-2}) in NaOH and different urea concentrations; (B) Transmittance measured *in situ* during voltammetry. [NaOH] = 1 mol L^{-1}; [urea] = 0, 10, 50, 150 and 300 mmol L^{-1}. Scan rate: 2 mV s^{-1}. Illumination: AM1.5G, 1000 W m^{-2}.

Figure 1

SEM plane view and cross-section images of Ti-Fe_2O_3 samples before (A) and after deposition of 2 nm of Ni by sputtering (B) or after NiOOH PEC deposition at 17.5 mC cm^{-2} (C). Scale bars: 100 and 200 nm for plan view and cross-section images, respectively. For cross-section imaging, metallization with 2 nm of $Pt_{80}Pd_{20}$ was applied to avoid charge accumulation.

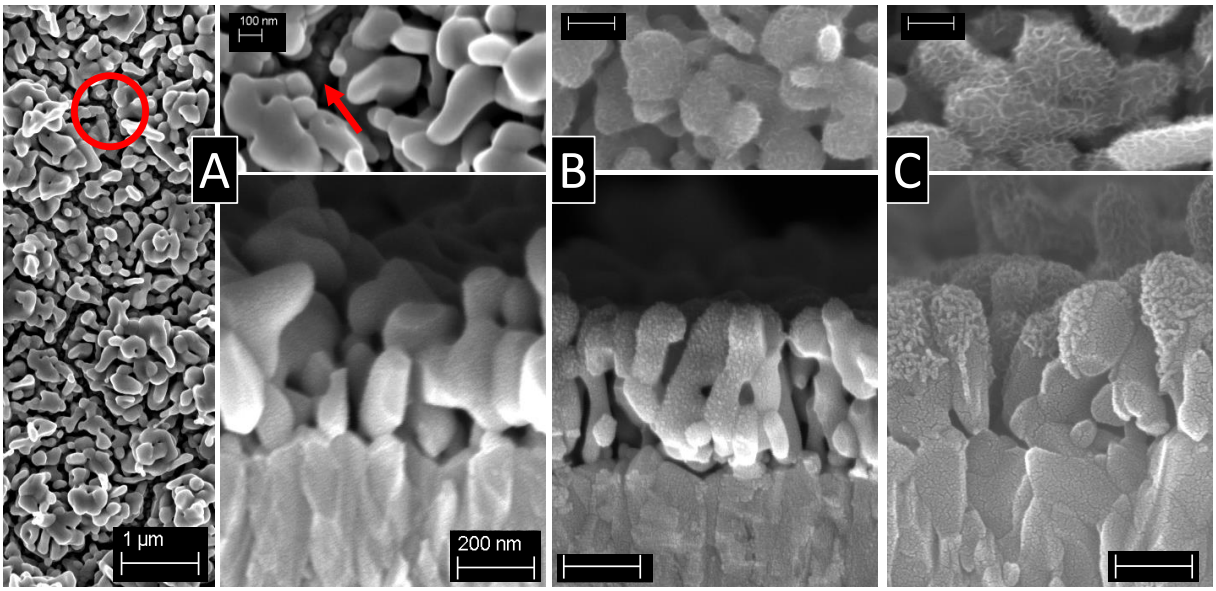

Figure 2

Absorptance and reflectance of FTO/Ti-Fe_2O_3 samples, with or without sputtered Ni (2 nm, A) and PEC deposited Ni (8.75 mC cm^{-2}, B). The dashed line at 590 nm corresponds to the gap of Fe_2O_3 (2.1 eV).

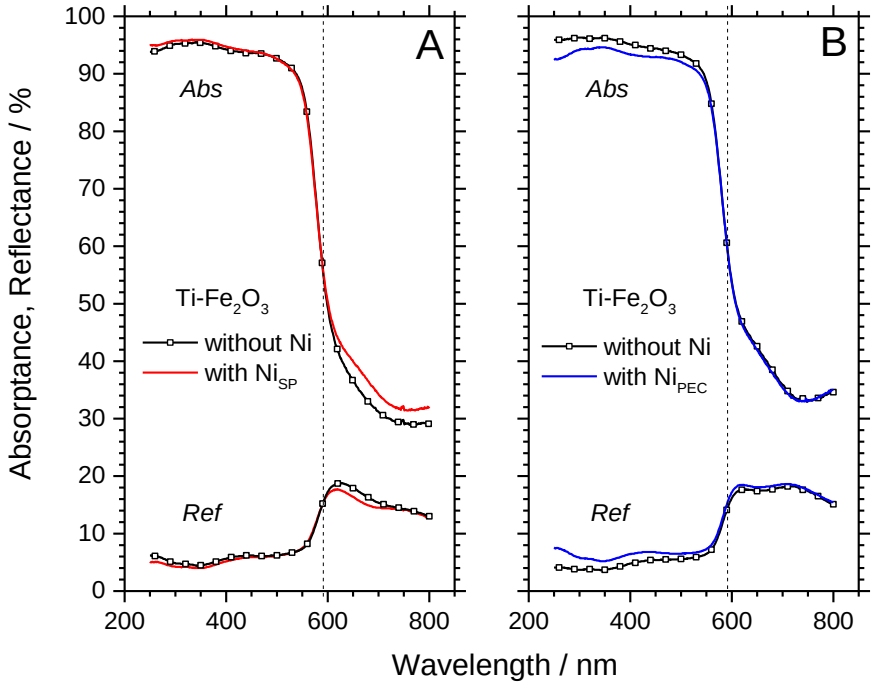

Figure 3

Voltammetry in the dark and under illumination of (A) FTO/Ti-Fe_2O_3 in NaOH, before and after sputtering deposition of 2 nm of Ni (Ti-Fe_2O_3/Ni_{sp}); (B) Ti-Fe_2O_3/Ni_{sp} in NaOH with or without urea. Table: Photocurrent values of both FTO/Ti-Fe_2O_3 and Ti-Fe_2O_3/Ni_{SP} electrodes at 1.23 et 1.40 V_{RHE}. [NaOH] = 1 mol L^{-1}; [urea] = 0.33 mol L^{-1}. Scan rate: 10 mV s^{-1}. Illumination: AM1.5G, 1000 W m^{-2}.

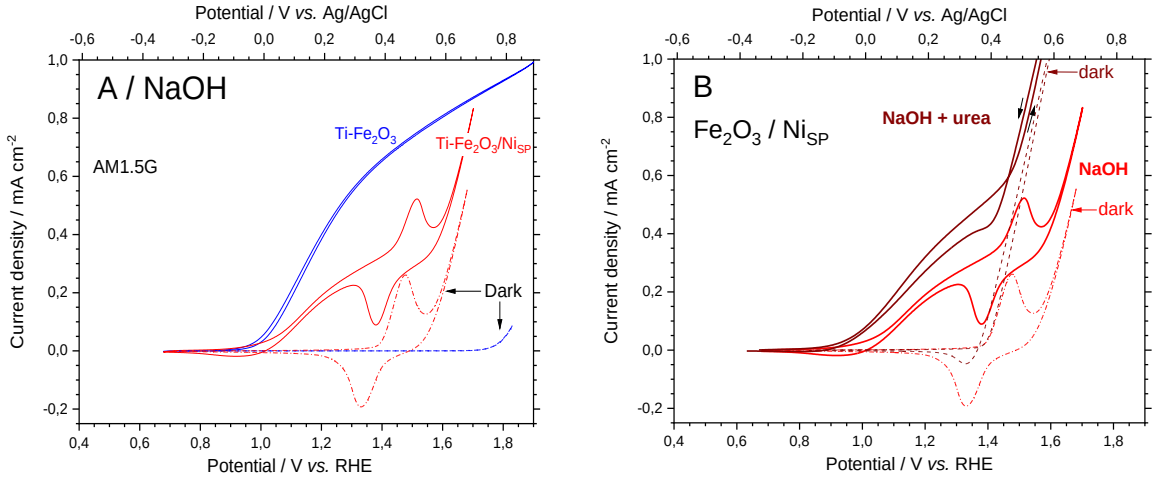

		NaOH (Fig. A)		NaOH + urea (Fig. B)	
	E / V_{RHE}	1.23	1.40	1.23	1.40
J_{ph} mA cm^{-2}	Fe_2O_3	**0.45**	**0.66**	**0.45**	**0.66**
	Fe_2O_3/Ni_{SP}	**0.22**	**0.29**	**0.35**	**0.47**

Figure 4

Voltammetry in the dark and under illumination of (A) FTO/Ti-Fe_2O_3 in NaOH, before and after PEC deposition of NiOOH (8.75 mC cm^{-2}); (B) Ti-Fe_2O_3/Ni_{PEC} in NaOH, with or without urea; (C) FTO/Ti-Fe_2O_3/Ni_{SP} and FTO/Ti-Fe_2O_3/Ni_{PEC} in NaOH with urea (under illumination only). Table: Photocurrent values of both FTO/Ti-Fe_2O_3 and Ti-Fe_2O_3/Ni_{PEC} electrodes at 1.23 et 1.50 V_{RHE}. [NaOH] = 1 mol L^{-1}; [urea] = 0.33 mol L^{-1}. Scan rate: 10 mV s^{-1}. Illumination: AM1.5G, 1000 W m^{-2}.

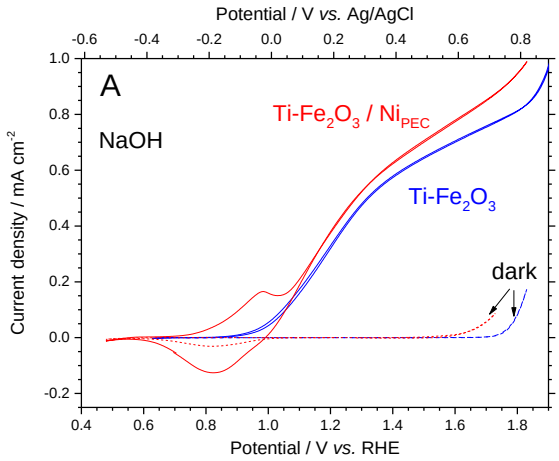

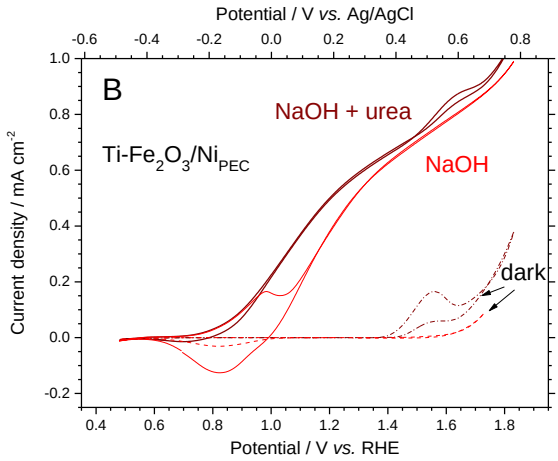

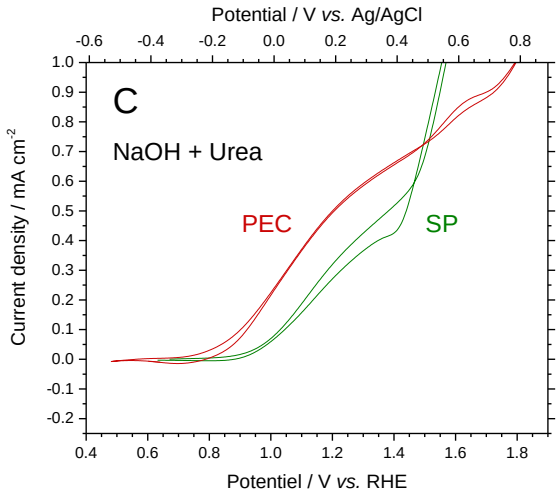

		NaOH (Fig. A)		NaOH + urea (Fig. B)	
	E / V_{RHE}	1.23	1.50	1.23	1.50
J_{ph} mA cm^{-2}	Fe_2O_3	**0.45**	**0.65**	**0.45**	**0.61**
	Fe_2O_3/Ni_{PEC}	**0.43**	**0.71**	**0.53**	**0.69**

Figure 5

(A) Voltammetry under illumination of FTO/Ti-Fe_2O_3/Ni_{SP} (2 nm) in NaOH and different concentrations of urea, with an insert showing the photocurrent onset potential region; (B) Transmittance measured *in situ* during voltammetry. [NaOH] = 1 mol L^{-1}; [urea] = 0, 10, 50, 150 and 300 mmol L^{-1}. Scan rate: 2 mV s^{-1}. Illumination: AM1.5G, 1000 W m^{-2}.

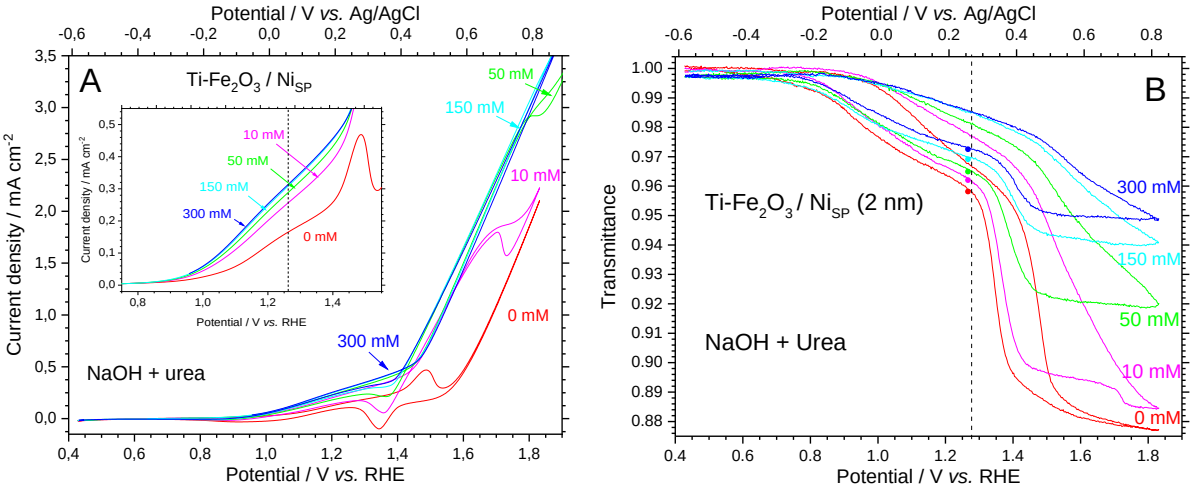

Figure 6

(A) Voltammetry under illumination of FTO/Ti-Fe_2O_3/Ni_{PEC} (8.75 mC cm^{-2}) in NaOH and different urea concentrations; (B) Transmittance measured *in situ* during voltammetry. [NaOH] = 1 mol L^{-1}; [urea] = 0, 10, 50, 150 and 300 mmol L^{-1}. Scan rate: 2 mV s^{-1}. Illumination: AM1.5G, 1000 W m^{-2}.

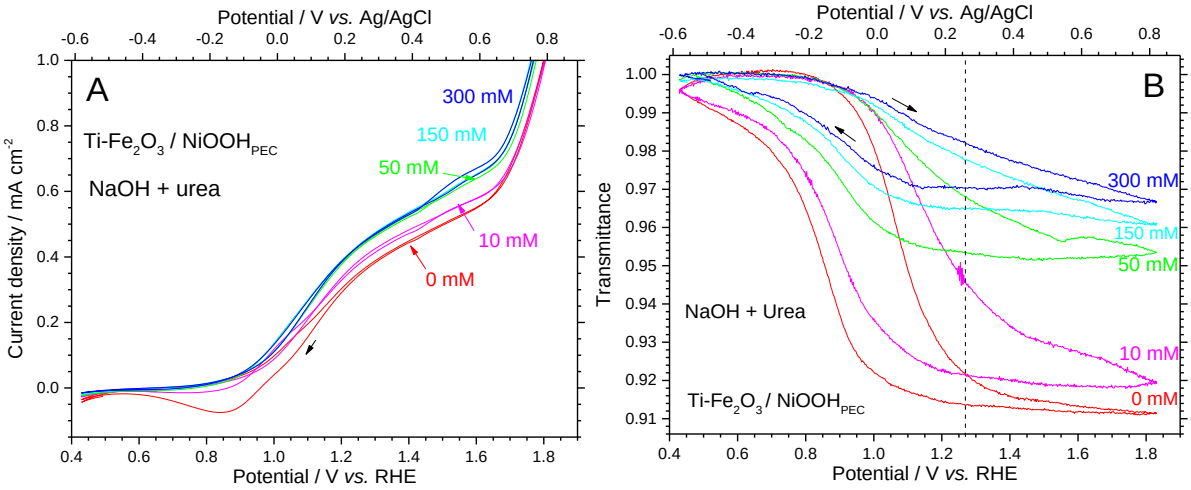

Photoelectrocatalytic conversion of urea under solar illumination using Ni decorated Ti-Fe_2O_3 electrodes

Lamia Rebiai *et al.*

TABLE

Table 1. Faradaic yields of products formed in the gas and liquid phase during four photoelectrolysis with FTO/Ti-Fe_2O_3/Ni_{PEC} of a 0.33 mol L^{-1} urea solution in 1 mol L^{-1} NaOH at 1.51 V_{RHE} during 4 h.

electrolysis		O_2		N_2		NO_2^-		Σ (calculated charges) /Total charge (%)
	Total charge (C)	calculated charge (C)	yield (%)	calculated charge (C)	yield (%)	calculated charge (C)	yield (%)	
E1	23.2	3.1	13.3	2.3	10.0	/	/	23.2
E2	25.3	8.9	35.0	2.8	11.1	/	/	46.3
E3	25.0	2.3	9.3	4.4	17.6	/	/	26.8
E4	**27.2**	**4.0**	**14.8**	**4.7**	**17.3**	**17.4**	**64.9**	**96.0**
Average	25.2 ± 2	4.6 ± 4	18.1 ± 12	3.6 ± 1	14.0 ± 4	/	/	/

Photoelectrocatalytic conversion of urea under solar illumination using Ni decorated Ti-Fe_2O_3 electrodes

Lamia Rebiai et al.

Highlights

- Urea conversion with Fe_2O_3/Ni photoelectrodes as substitute for N-removal in WWTPs
- Anodic photoelectrodeposition of NiOOH on n-Fe_2O_3 nanorods where h^+ are collected
- Gain of 0.5 V in urea oxidation onset potential with FTO/Ti-Fe_2O_3/Ni *vs.* Ni electrode
- *In situ* light transmission recorded during CV confirms urea oxidation as EC process
- Urea PEC conversion leads to N_2, O_2, and NO_2^- ; FE ~ 10-20% for N removal as N_2